An investigation on the impact of small scale models in Gasoline Direct Injection sprays (ECN Spray G).

Journal Title
XX(X):1–8

DOI: 10.1177/ToBeAssigned
www.sagepub.com/
SAGE

Salvador Navarro-Martinez[1], Giovanni Tretola[1], Mohammadreza Yosri[2], Robert Gordon[2], Konstantina Vogiatzaki[3]

Abstract

The work presents a numerical investigation of gasoline direct injection and the resulting early development of spray plumes from an 8-hole injector (ECN Spray G). The objective is to evaluate the impact on the droplet size distribution statistics from the assumed model physics, particularly for the small scales. Two modelling approaches are compared: Eulerian-Lagrangian Spray Atomisation with Adaptive Mesh Refinement (ELSA-AMR) and a stochastic fields transported-PDF method (ELSA-PDF). The two models simulate the small scales and sub-grid droplet physics with different approaches, but based on the same concept of transport of liquid surface density. Both approaches predict similar liquid distributions in the near-field comparable to experimental measurements. The spray breakup patterns are very similar and both models reproduce quasi log-normal droplet distributions, with same overall Sauter Mean Diameters. The ELSA-PDF approach shows a different break-up behaviour in droplets originating from the dilute region and those originating from the dense core region. The transition from Eulerian to Lagrangian can be observed in the ELSA-AMR predicted distribution with an abrupt change in the droplet size distribution. Both methods are able to produce similar droplet size distributions below filter width/grid size resolution.

Keywords

Eulerian-Lagrangian Spray Atomisation, fuel sprays, droplet break-up models, stochastic fields methods, Engine Combustion Network (ECN) Spray G

Introduction

The challenges of characterising sprays in internal Combustion (IC) engines has resulted in a technological bottleneck in the development of a new generation of, low carbon and low soot, efficient engines. In the year 2017, more than half of all new cars and approximately half of light truck sales feature Gasoline Direct Injection (GDI) systems[1] and this market share will continue to increase as manufacturers introduce more advanced engines into the market. The successful implementation of a GDI system requires a thorough understanding of the fuels behaviour in-cylinder. The fuel distribution has a significant impact on the subsequent combustion and the emissions outputs of the engine. Modelling the complete spray atomisation process is challenging, as different liquid-gas break mechanisms occur in different parts of the spray system. Recent developments in break-up models recently have focused on droplet fragmentation and ”secondary” break-up models. Such approaches assume the droplets are isolated, subject to either capillary or shear flow instabilities.

In GDI injectors, the large jet exit velocity combined with the presence of bore holes can create compressible effects (cavitation, hydraulic flip). These effects, in turn, can affect the flow near the nozzle and the subsequent liquid break-up. GDI injectors combine dense liquid regions, where break-up is produced by ligament forming processes, and dilute regions where liquid break-up occurs at a different scale. Computational models that accurately solve the interphase boundary, such as Volume-of-Fluid (VOF), Level-Set or similar methods, are very expensive in the range of Weber numbers that GDI injectors operate. Unpractical meshes of several billion grid points are required if the near-field breakup is to be resolved accurately. The cost of the simulation will also increase if phase-change and compressible effects are also to be included.

A new intermediate class of methods have been growing in popularity based on the concept of modelling the liquid surface density. These methods, often called Eulerian-Lagrangian Spray Atomization (ELSA) models[2], or $\Sigma - Y$, solve equations for the liquid volume and the surface density. These variables provide *local* information on the size of liquid fragments, in scales that are smaller than the computational cells. The ELSA equations can be solved in a Reynolds Average Navier-Stokes (RANS) context, or Large Eddy Simulations (LES) where the better description of turbulence may improve the predictions. The information at the small scales can provide the initial condition to

[1]Department of Mechanical Engineering, Imperial College London, UK
[2] Department of Mechanical Engineering, The University of Melbourne, Australia
[3]Advanced Engineering Centre, University of Brighton, UK

Corresponding author:
Salvador Navarro-Martinez, Department of Mechanical Engineering, Imperial College London, SW7 2AZ, UK.
Email: s.navarro@imperial.ac.uk

"inject" droplets when the spray becomes diluted. A new Lagrangian description framework is then established and droplets are tracked as points in a turbulent flow. Different ELSA approaches model the generation and destruction of the liquid surface slightly differently. This can lead to discrepancies in the production on the smaller droplet sizes and consequently the droplet size distribution.

The original RANS-based formulations[2,3] the destruction and generation terms have empirical coefficients, in particular if droplet collisions are considered. In more recent formulations in LES context[4,5], there is less uncertainty in the surface generated by turbulence the destruction term , but still in the small-scale effects of surface tension.

In this work, two ELSA approaches are compared: conventional ELSA[2] and ELSA-PDF[5]. These are implemented within two popular software packages, CONVERGE, from[6] and OpenFOAM, see for example[7]. CONVERGE implements Adaptive Mesh Refinement (AMR) to reduce the mesh and improves the resolution (hereafter ELSA-AMR). ELSA-PDF uses a stochastic approach to solve the joint surface/volume distribution at sub-cell (or sub-grid) scales.

The capabilities of these approaches are compared for a GDI injector (Spray G) from the Engine Combustion Network(ECN). Spray G is a suitable validation test case for models that represent the key physics. Despite the geometric complexity, the Spray G condition is non-flashing and mildly cavitating. Key aspects of the modelling of this injector have been previously explored,[8–12], such as the impact of in-nozzle geometry and transient needle lift. Flash-boiling effects have also be investigated numerically in the Spray G2 condition[13] (with lower ambient temperature) in the same injector. However, the characterisation of the near-field droplet distribution has not been reported nor the application of ELSA-PDF in a GDI.

In the next section, a brief description of the methodologies used is presented, follow by description of the experimental and numerical set-up, followed by the results.

Methodology

The multiphase dynamics are described in ELSA-approaches using two variables: the liquid volume fraction (or VOF), $\alpha(\mathbf{x},t)$, and the surface density $\Sigma(\mathbf{x},t)$, which represents the amount of liquid/gas interface per unit volume. α in some texts (and the default in CONVERGE)is often referred as void fraction. Through the remainder of this text $\alpha \equiv \alpha_{fuel}$ will be the liquid fraction and the output of converge will be re-defined to reflect this. The VOF transport equation can be obtained directly from the continuity equation as α is transported by the flow field. The Σ transport equation can be derived from surface dynamics within the flow; additional terms appear in to describe the generation/destruction of the surface, due to capillary effects, phase change and droplet collision.

These terms can be grouped with a general source/sink term: $S = S_{gen} - S_{des}$, where S_{gen} describes the generation of the surface due to flow field motions, and S_{des} corresponds to surface destruction from collision and capillary effects. The source term can be written as a non-linear restoration to equilibrium term[3]:

$$S(\alpha,\Sigma) = \frac{\Sigma}{\tau}\left(1 - \frac{\Sigma}{\Sigma_{eq}}\right) \tag{1}$$

where Σ_{eq} is an equilibrium surface density and τ is an associated relaxation time-scale[2] related to the flow[5]. At high Weber numbers typical of spray atomization, the time scale can be an LES-scale based on the filtered strain rate, $\tau \propto ||\bar{S}_{ij}||^{-1}$, or proportional to a turbulent time scale (as in RANS).

Capillary effects are restricted to Σ_{eq}, and a local equilibrium surface can be characterised by a critical Weber number following[14]: $We_{crit} = \rho k_{sgs}\alpha/\sigma\Sigma_{eq}$ where k_{sgs} is the local sub-grid turbulent kinetic energy. Critical number values of $We_{crit} = 1$ are often used, but higher values also are reported in the literature[3,14]. In RANS context, the value Σ_{eq} is obtained assuming that droplet collision is the main break-up mechanism[15]. In ELSA-LES formulations, there is no *a-priori* assumptions regarding the break-up mechanism, and closures are based on sub-grid equilibrium between surface and kinetic energy.

ELSA-AMR in CONVERGE

The ELSA-AMR approach used with CONVERGE is based on the solution of the Eulerian LES transport equations for liquid volume and surface density:

$$\begin{aligned} \frac{\partial\overline{\alpha}}{\partial t} + \bar{u}_j\frac{\partial\overline{\alpha}}{\partial x_j} &= \frac{\partial}{\partial x_j}\left(D_\alpha\frac{\partial\overline{\alpha}}{\partial x_j}\right) - S^*_\alpha \\ \frac{\partial\overline{\Sigma}}{\partial t} + \bar{u}_j\frac{\partial\Sigma}{\partial x_j} &= \frac{\partial}{\partial x_j}\left(D_\Sigma\frac{\partial\overline{\Sigma}}{\partial x_j}\right) + S(\overline{\Sigma},\overline{\alpha}) - S^*_\Sigma \end{aligned} \tag{2}$$

where D_α and D_Σ are sub-grid diffusivities, which are assumed to be proportional to the sub-grid viscosity with $D_\alpha = D_\Sigma = D_{sgs} = \nu_{sgs}/Sc_{sgs}$, where Sc_{sgs} is a turbulent Schmidt number taken as 0.9. The S^* represent the sink of liquid volume/surface due to transition to Lagrangian and mass change effects following Pandal Blanco's approach[16] (see CONVERGE manual[6] for details). To account for the phase/change due to cavitation, and Homogeneous Relaxation Model (HRM) is employed[17].

The transition from the Eulerian to the Lagrangian field is produced when the local liquid volume fraction is smaller than an imposed transition value $\overline{\alpha} < \alpha_{tr}$ and surface is still present, $\Sigma > \Sigma_{min}$. Using a large transition value, the potential for transition from the Eulerian-to-Lagrangian field increases as well as the number of parcels. In this work $\alpha_{tr} = 0.9$, following Saha *et. al.*[12]. The diameter of the spherical droplet introduced is $d = \alpha/\Sigma$ and the corresponding liquid mass is remove from the Eulerian phase. Several droplets with the same diameters and properties can be grouped in "parcels" to save computational time.

ELSA-PDF in OpenFOAM

The ELSA-PDF approach employed in the present work is based on solving the joint probability density function (PDF) of scalar and surface density. From the PDF transport equation (not shown, see Navarro-Martinez[5] for details)

an equivalent system of Stochastic Partial Differential Equations (SPDE) can be derived using N stochastic fields, where each stochastic field has its own volume fraction and surface density, α^n and Σ^n respectively.

Following the Ito formulation[18], the transport equations for the stochastic fields are:

$$\begin{aligned}\frac{d\alpha^n}{dt}+\bar{u}_j\frac{\partial\alpha^n}{\partial x_j}=&\\ \frac{\partial}{\partial x_j}\left(D_{sgs}\frac{\partial\alpha^n}{\partial x_j}\right)+\sqrt{2D_{sgs}}\frac{\partial\alpha^n}{\partial x_j}\frac{dW_j^n}{dt}&\\ \frac{d\Sigma^n}{dt}+\bar{u}_j\frac{\partial\Sigma^n}{\partial x_j}=\frac{\partial}{\partial x_j}\left(D_{sgs}\frac{\partial\Sigma^n}{\partial x_j}\right)&\\ +\sqrt{2D_{sgs}}\frac{\partial\Sigma^n}{\partial x_j}\frac{dW_j^n}{dt}+S(\Sigma^n,\alpha^n)&\end{aligned} \tag{3}$$

where D_{sgs} is the sub-grid diffusivity, proportional to the sub-grid viscosity $D_{sgs}=\nu_{sgs}/Sc_{sgs}$ obtained by the LES solver (with $Sc_{sgs}=0.9$), $d\mathbf{W}^\phi$ represent a Wiener process with mean 0 and variance equal to $\sqrt{dt}$. The solution for the system of SPDEs represents an equivalent system to the PDF equations. The first-moments (or filtered values) are obtained directly by averaging the Stochastic Fields solution

$$\bar{\alpha}=\frac{1}{N}\sum_{n=1}^{N}\alpha^n \tag{4}$$

The averaged Equation (3) will be equivalent to the LES counterpart 2 After the stochastic field equations have been advanced, all relevant parameters can be obtained directly. For example, the characteristic fragment length per stochastic field is the Sauter Mean Diameter (SMD) defined as

$$d_{32}^n=6\frac{\alpha^n}{\Sigma^n} \tag{5}$$

where the corresponding filtered moments, $\bar{d}_{32}$, can be obtained directly through Eqn. (4). Local Droplet Size Distributions can be obtained directly from binning the SMD. Although a transition to Lagrangian droplets could be performed in a similar way as ELSA-AMR, no Lagrangian transition is implemented in this work within ELSA-PDF.

Spray G Set-up

The experimental set-up consists of an eight-hole counter-bore GDI fuel injector, denoted as the Spray G nozzle in the Engine Combustion Network[19]. The nozzle geometry and spray conditions were determined from the selected ECN experimental test case. The spray system consists of an 8-hole nozzle, with a fuel injection pressure of 200 bar and a nozzle diameter of 170 microns (with an uncertainty of 1.8 micron). The internal geometry is not symmetric, and differences in the flow patterns are expected across the holes, that create different discharge coefficients. The fuel is taken as iso-octane at a temperature of 363 K. The injected mass is 10 mg over 780 μs. The computational domain is based on the ECN setup of the in-nozzle geometry and a 3mm domain extent, or cap. The needle is set at the fully open position with a gap of 50 μm. The coordinate $z=0$ corresponds to the top. of the cylinder, with $z>0$ inside the cylinder.

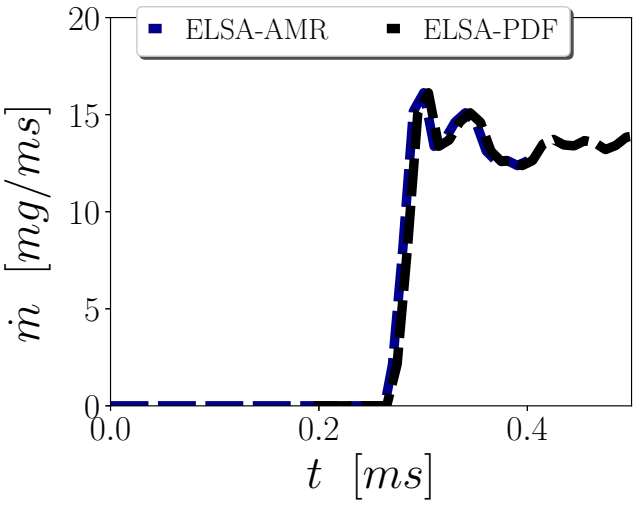

Figure 1. Mass flow rate for ELSA-AMR and ELSA-PDF.

To represent the experimental needle lift, a mass flow profile is used following the recommended mass flow profile of the ECN Workshop on Spray G. This set-up has been used previously to model Spray-G, with good agreement on spray penetration[12]. Both the ELSA-PDF and ELSA-AMR approaches use the same inflow boundary conditions, and a zero-gradient is used as the outflow boundary condition for the cap. Baldwin *et al.*[13] show that using moving meshes and accounting for compressibility approaches could capture the flow pattern in Spray G. Alternatively, Saha *et al.*[12] use an incompressible formulation approach and the latter approach is followed.

Figure 1 shows the mass flow rate for ELSA-AMR and ELSA-PDF. The time when the $\dot{m}>0$ defines the time 0, for each simulation, for the definition of the liquid penetration. The simulation time is approximately 30 μs after the fluid exits the nozzle. This time is short enough so effects of the needle wobble and overshoot can be ignored. A summary of the conditions can be found in Table 1.

Table 1. Spray G conditions[19] and simulation parameters

	OpenFOAM	CONVERGE
Upstream Pressure	200 bar	200 bar
Fuel Temperature	90°	90°
Ambient Temperature	300°	300°
Back pressure	6 bar	6 bar
Simulation time	30μs	30μs
Phase Change	no	yes
Compressible Flow	no	no
Grid	structured	AMR
Smaller cell-size	5μm	4.7μm

Both CONVERGE and OpenFOAM use the finite volume method to solve the conservation equations. CONVERGE uses a second order flux blending scheme for spatial discretisation[6] together with a PISO algorithm[20] to solve the pressure-momentum coupling. The dynamic structure model is implemented to model the sub-grid stress term[21]. OpenFOAM[7] uses second order central flux schemes and similar PISO pressure solver as CONVERGE. A correction procedure is performed for α and Σ, to avoid excessive

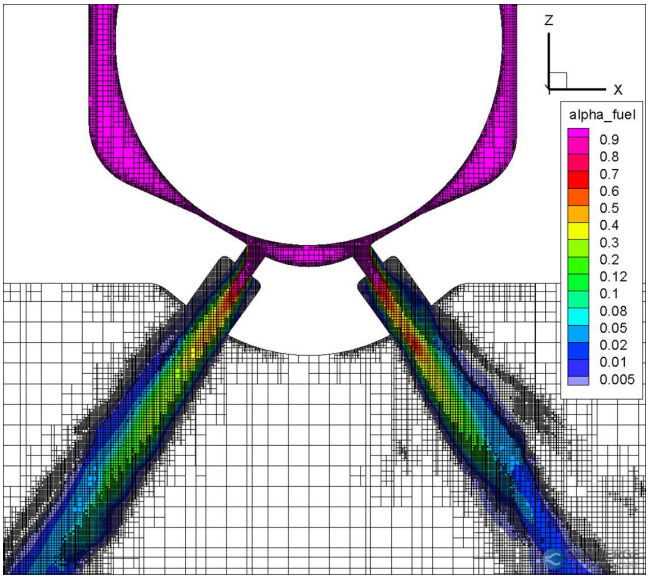

Figure 2. Detail of the mesh generated by CONVERGE close to the nozzle

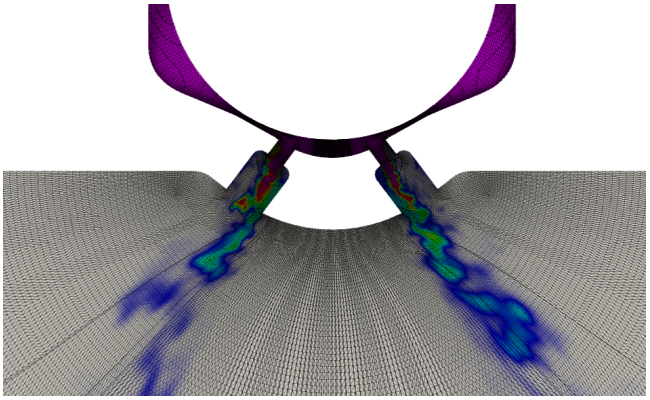

Figure 3. Detail of the mesh generated by OpenFOAM close to the nozzle

numerical diffusion and guarantee scalar bounds. A WALE turbulence model[22] determines the sub-grid viscosity ν_{sgs}, required for the sub-grid stresses and turbulent transport. $N = 16$ stochastic fields are used to describe the sub-grid PDF in line with previous works[23]. The number of samples is relatively low and the Monte-Carlo statistical errors scale with $\sigma_{sgs}/\sqrt{(N)}$, where σ_{sgs} is the sub-grid variance. A sub-grid variance $\sigma_{sgs} \approx 5\%$ will introduce a local *instantaneous* sampling error of 1% with 16 stochastic fields. However, time or spatially averaged results will have a much larger sample and statistical errors will be small. Increasing the number of fields to 64 can improve marginally the sub-grid PDF description, however the larger cost offsets the benefits.

The AMR algorithm embeds new cells in the mesh where the sub-grid velocity fluctuations are above a threshold ($0.5m.s^{-1}$ in this case), and cells are coarsened where the sub-grid velocity fluctuations are below $1/5^{th}$ of this value. See Figure 2.

The base grid size at its coarsest level has cells of $0.15\ mm$ and the smallest cell size is approximately 4.7μm. The grid resolution is finer than the previous Spray G simulation of Saha *et al.*[9,12], where the finest mesh was 125 μm (centred

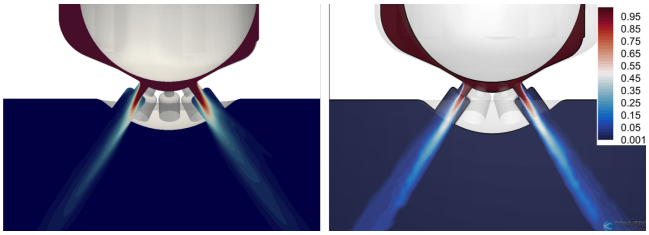

Figure 4. Vertical section of: time-averaged $< \alpha >$; ELSA-PDF OpenFOAM (left) and ELSA-AMR (right);

on the far field) and 15 μm, while Baldwin *et al.*[13] used a refined mesh with minimum size of 7μm.

A variable time step is calculated based on the maximum convection 0.3) and diffusion CFL number (2.0), and ranges from $0.6 - 50ns$. The maximum number of cells was limited to ten million. However, the number of Lagrangian parcels increases with time, reaching 38 million over the simulation,

The OpenFOAM simulation used a conventional curvilinear structured mesh provided by the ECN Workshop[19] and generated with GridPro (see details in Fig. 3). The mesh consists of 5.5 million cells, with a minimum size of 5 μm in the needle tip and nozzle and an average size of 10 μm in the counter-bore. The maximum cell size is 65 μm approaching the domain exit. The Taylor length scale can be estimated (for singe phase flow) $\lambda/D \approx \sqrt{10}Re^{1/2}$, which gives an estimate at the nozzle exit of 1.2 μm. Both approaches have mesh-to-Taylor lengths scale ratios of 4-5, which suggests that while the mesh is far from DNS resolution, the resolution is adequate for LES of jet flows.

The meshes employed in both approaches have sufficient resolution to capture the initial shear layer at the nozzle exit. The response of the LES models between the approaches may be different; The sub-grid viscosity in ELSA-AMR will be smaller (due to local refinement) than ELSA-PDF. Nevertheless, if the filtered gradients are well captured, the turbulence response should be the same and differences outside the nozzle can be attributed to the different ELSA implementations.

Results

This section aims to understand the similarities and differences between the two approaches. Through these differences, the role of the small scales will be highlighted.

Figure 4 shows the time-averaged volume fraction, α, between the two methods. Although, α is associated in CONVERGE with the void-fraction, the output of converge has been modified to provide the liquid volume fraction and therefore provide a more meaningful comparison between models. In the region where $\alpha \geq 0.25$ the two approaches present similar distributions: the fuel exits the nozzles, filling only one side of the counter-bores. This was observed previously in the literature[8,13]. Differences are observed outside the nozzle: the side close to the wall presents a small volume fraction for ELSA-PDF, while ELSA-AMR in CONVERGE shows no liquid. In this part of the counter-bore, a pressure lower than the saturation one exits, and cavitation should be expected. Phase-change is not considered in ELSA-PDF, however it is accounted in ELSA-AMR. Figure 5 reports the iso-octane vapour distribution

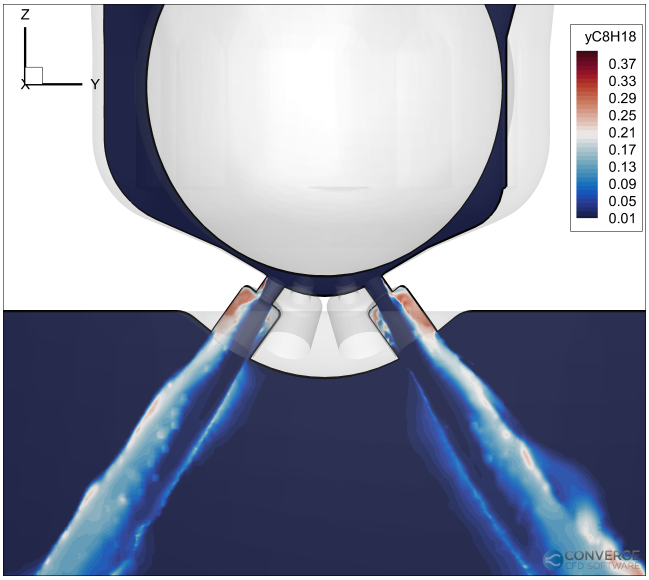

Figure 5. vertical section of iso-octane vapour mole fraction distribution, ELSA-AMR.

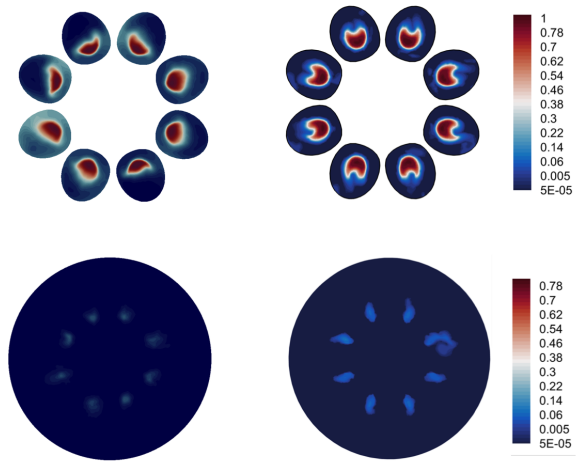

Figure 6. Snapshot of time-averaged α across the injection holes at: $z = 0$ **top** and $z = 2$ mm **bottom**. ELSA-PDF (left), ELSA-AMR (right). Legend as in Fig. 4.

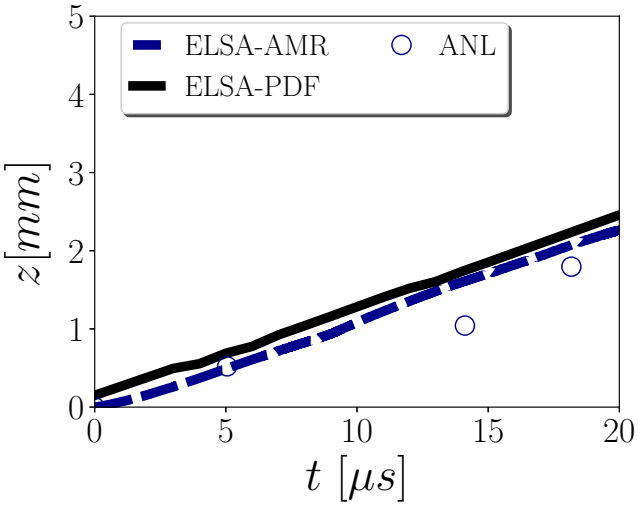

Figure 7. Predicted liquid penetration compared with experimental data,[19]. Domain limit, z_{max}, in both simulations is 3 mm .

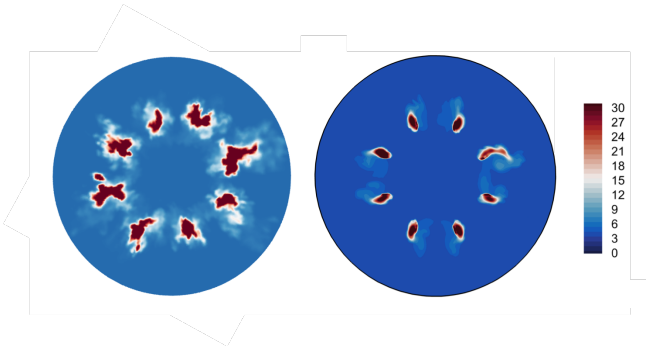

Figure 8. Density field (units $\mu g/\text{mm}^3$) in $x - y$ plane at $z = 2$ mm : **(left)** ELSA-PDF and **(right)** ELSA-AMR.

obtained with ELSA-AMR, the vapour generated by cloud cavitation, combined with the rapid generation of fine droplets accounts for the sharp decay of liquid in the counter-bore.

Once the liquid fuel exits the holes, $\alpha \leq \alpha_{tr}$ and the Eulerian liquid description transitions to Lagrangian spherical droplets in CONVERGE. The amount of liquid in the Eulerian phase reduces and a few diameters downstream the concentration is very small. The ELSA-PDF is a full Eulerian approach and does not transition to a Lagrangian phase within the domain, therefore the liquid volume fraction is more continuous.

Figure 6 shows the distribution of $\langle\alpha\rangle$ on a transverse plane $x - y$ at two different distances: the first at $z = 0$, which corresponds to inside the counter-bored holes, and the second is 2 mm downstream, once the spray is formed. The asymmetry of the injector is clearly seen in the flow, through the non-symmetric liquid pattern. This is due to the asymmetric geometry of the Spray G nozzle, which consists of eight holes and five dimples. ELSA-PDF shows some of the holes "filled" with liquid, while cavitation and Lagrangian transitions in ELSA-AMR shows significant upstream penetration of gas in nearly all holes. The effect of cavitation seems limited to the counter-bore, and it does not significantly affect the spray, as evidenced by the similar patterns in both simulations. The experimental data of Duke[24] is qualitatively similar, however its data is averaged over 700μs and cannot be quantitatively compared.

Figure 7 shows the liquid penetration in both approaches, taken as the position where the liquid volume fraction $\alpha \geq 0.1$. The time starts from the instant where the liquid exits from the counter-bore. The liquid penetration follows the same linear trend as the experimental data, with slightly higher gradients. Over these early stages of injection, the liquid penetration follows the injected mass flow rate profile.

Figure 8 shows the density field, ρ, on an $x - y$ plane at $z = 2$ mm, as reported Duke *et al.*[24]. In ELSA-AMR the density observed is close to the one reported in literature, while the ELSA-PDF model predicts a wider central core of density due to the absence of phase-change in the method. As reported by Baldwin *et al.*[13], compressible effects are required to correctly predict the density distribution within the bores.

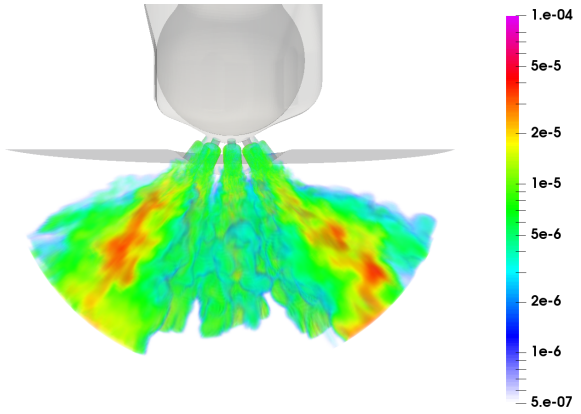

Figure 9. Instantaneous distribution of the droplet Sauter Mean Diameter ($d32$), ELSA-PDF at $t = 150\mu s$.

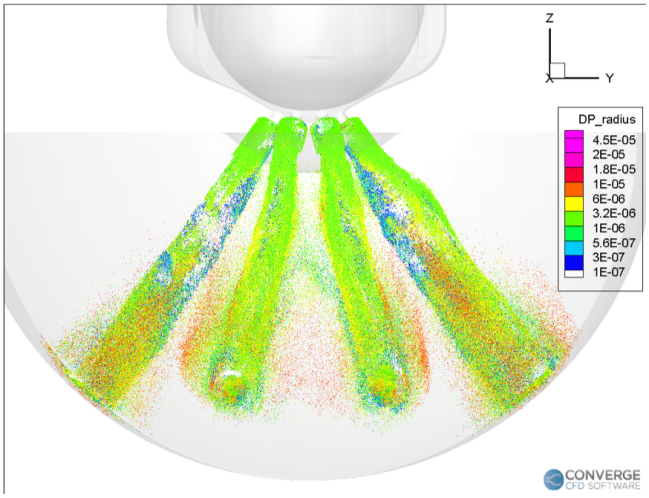

Figure 10. Instantaneous distribution of the Lagrangian transported droplets, ELSA-AMR at $t = 104\mu s$.

Figures 9 and 10 show instantaneous distributions of the droplet Sauter Mean Diameter ($d32$ in ELSA-PDF) and Lagrangian droplets coloured by size (in ELSA-AMR). Both figures show similar patterns, with a core of large droplets of order 10-20 μm in ELSA-AMR and 20-40 μm in ELSA-PDF. The droplets in the Lagrangian context show lower dispersion due to the initial velocity provided to them at "generation" close to the nozzle from their local gas velocity. Particle dispersion and drag models can be inaccurate in this region, where turbulence gradients may not be well resolved and the assumption of spherical droplets. The breakup model, Kelvin-Helmholtz Rayleigh-Taylor (KH-RT)[25], is also known to favour the creation of small droplets, as every droplet breaks into half or a third on breakup. Eulerian approaches do not have the restriction of spherical droplets, but account for only one mixture velocity, and do not permit liquid/gas slip velocities, all of which would affect the droplet dispersion and turbulence modulation.

The major advantage of the ELSA methodology is the prediction of the droplet-size distribution without the need of an *a-priori* break-up model.

The predicted distribution is observed in Figure 11 for the ELSA-PDF. Using fifty bins of constant size in the range $[0 - 50\mu\text{m}]$, a histogram is computed from sampling droplets outside the counter-bores. A normalised droplets distribution can be then extracted and log-normal fits (with same mean and variance from the sampling data) are also shown for comparison. A threshold value of $\alpha = 0.1$ has been selected to arbitrarily distinguish between dense and dilute regions.

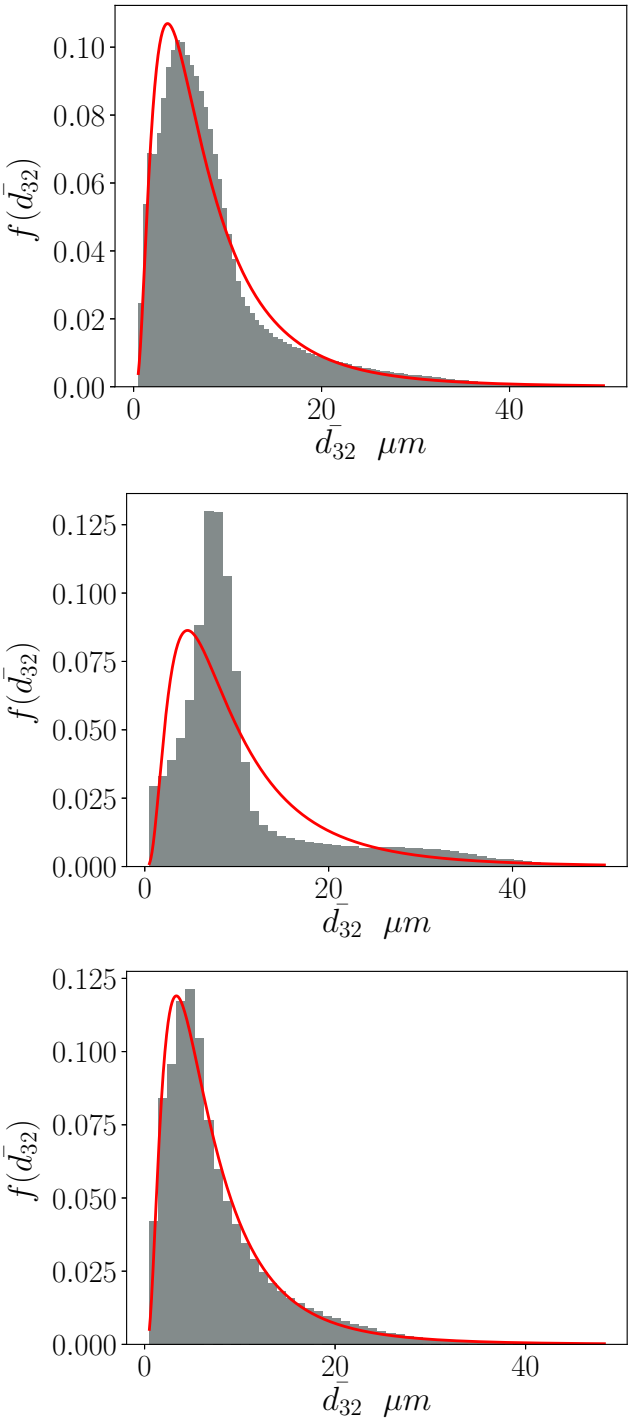

Figure 11. Normalised Droplet size distribution: (top) whole domain, (centre) dense $\alpha > 0.1$, (bottom) dilute $\alpha < 0.1$. The solid line indicates log-normal distribution with same mean and variance of sampled distribution.

The droplet size distribution over the whole domain has a mode of approximately 4.5 μm, with a mean of 8.5 μm and a standard deviation of 7.5 μm. The overall distribution fits a log normal profile with the same mean and variance. Nevertheless, when only the dense region is considered,

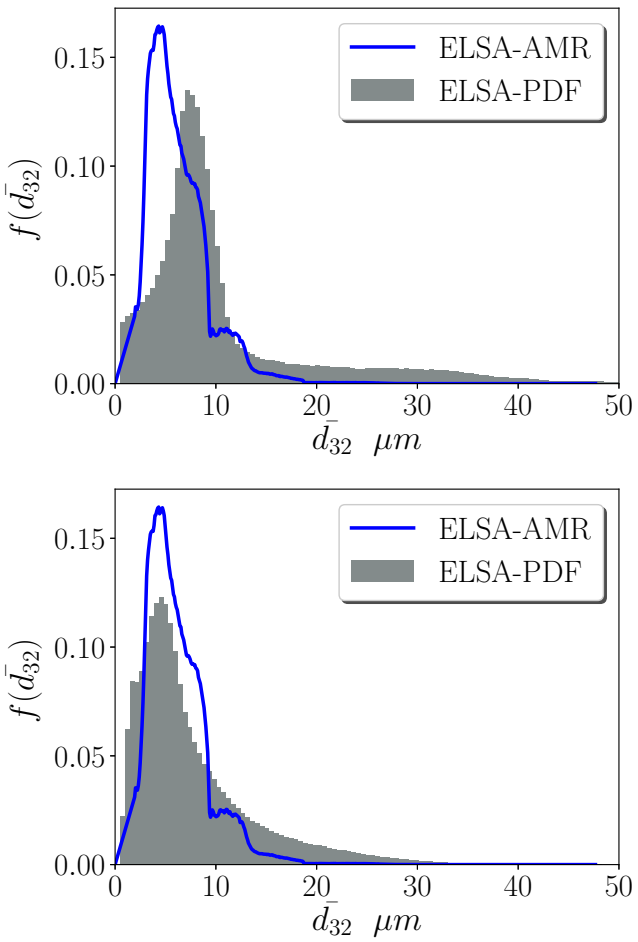

Figure 12. Droplet size distribution from ELSA-AMR and ELSA-PDF **(top)** $\alpha > 0.1$ dense, **(bottom)** $\alpha < 0.1$ dilute.

the distribution is markedly different: The predicted mode, mean and the variance are larger (7.0μm, 10.5μm and 9μm respectively) and the shape of the distribution does not follow a log-normal distribution. There is also sharp decay and a long tail of large liquid fragments, up to 40μm. When only the droplets present in dilute regions are considered, $\alpha < 0.1$, the distribution follows almost exactly a log-normal, with mode, mean and standard deviation of 4.3μm, 7.7μm and 6μm respectively. This suggests that the droplet break-up is controlled by the dilute region, which surrounds the dense core (see Fig. 4). The log-normal distribution appears naturally in processes with constant fragmentation rates. This will suggest that the rate of droplet formation in the dilute region is quasi-homogeneous and controlled by the local turbulence (or strain-rate). The dense region, $\alpha < 0.1$, creates large non-spherical fragments which have non-homogeneous fragmentation rates, creating the deviation from log-normal distribution.

Figure 12 compares the droplet size predicted by sampling (in ELSA-PDF) and the droplet sizes observed in the Lagrangian approach in ELSA-AMR. It is not possible in the ELSA-AMR results to distinguish between droplets in dilute or dense regions, and only one set of results is reported.

The results predicted by CONVERGE present a narrow distribution, with a sharp cut-off at 10μm and almost no droplets are predicted larger than 20μm. The transition criterion, α_{tr}, has an effect on the SMD[12] and the number of parcels. Large α_{tr}, produced larger initial droplets and increase the parcel count. These differences will diminish later as secondary Lagrangian Break-up models (such Rayleigh-Taylor in CONVERGE) will quickly fragment large droplets and reduce SMD. As previously noted, the Rayleigh-Taylor break up model breaks the droplets into half (or less), and thus creates a rapid reduction in droplet size.

Overall, distributions for both approaches are similar in the small scales, and differences are observed in the largest of the small-scales ($10 - 20\mu$m ranges). This size is the most difficult to predict as: a) droplet size are comparable to mesh size and Lagrangian coupling approaches are less accurate b) the assumption of spherical droplets inherent in Lagrangian approaches may not be applicable so close to the injector, where ligaments and non-spherical liquid fragments may be expected.

Table 2 shows SMD comparison between both approaches and exiting literature results[12] after the initial transient. The results show that overall both ELSA approaches show the same SMD (and are close to previous ELSA-RANS[12]) .

The mildy cavitating effects at the bore, do not seem to have an effect in the produced droplets, and only low-probability, large droplets seem to be affected. The smooth DSD distribution of ELSA-PDF suggest that, *a-priori*, it would be possible to delay the transition to a Lagrangian formulation and reduce the number of parcels by sampling from ELSA-PDF distributions.

Table 2. Most probable SMD at end of simulation.

ELSA-RANS[12]	5μm
ELSA-AMR	4.5μm
ELSA-PDF	4.5μm
ELSA-PDF , $\alpha > 0.1$	7μm
ELSA-PDF , $\alpha \leq 0.1$	4.3μm

Conclusions

In this work, two ELSA approaches have been tested in the near field of a GDI injector (Spray G). Both approaches predict an overall similar liquid distribution in the near field of Spray G, with asymmetric liquid distribution as well as hole-to-hole variation. The ELSA-AMR approach predicts the appearance of iso-octane vapour within the bores, which affect the flow patterns within the chamber. In the present configuration, ELSA-AMR appears to have the better agreement with the experimental measurements.

Outside the holes, both approaches reproduce the experimentally observed penetration. The ELSA-AMR approach transfers the Eulerian information to a set of Lagrangian droplets, the subsequent dispersion produces a smaller spray angle than the Eulerian solution.

Despite the near-field discrepancies, the break-up patterns are similar, and both models reproduce a quasi log-normal distribution of sub-grid droplets, predicting median droplets sizes with less than 10 % difference. The ELSA-PDF approach distinguish between the dilute spray regions which follow a log-normal distribution, and the dense core where larger fragments are formed and a log-normal distribution cannot be observed. In the ELSA-AMR approach, the Eulerian-to-Lagrangian transition can be observed in the

drop in the distribution for droplets larger than 10 μm, and droplets bigger than 20 μm are not found. Overall, both methods are able to produce similar droplet size distributions below filter width/grid size resolution. These obtained distributions can be used delay the transition to the Lagrangian treatment of the droplets and therefore reduce the complexity and cost of the simulations.

Acknowledgements

This work is part of the HAoS project, which is supported by the EU as part of the Horizon 2020 program. The authors also acknowledge funding by the UK's Engineering and Physical Science Research Council support through the grant EP/P012744/1 (KV).

References

1. Agency UEP. The 2018 EPA Automotive Trends Report. Technical report.
2. Vallet A, Burluka AA and Borghi R. Development of an eulerian model for the atomization of a liquid jet. *Atomization and Sprays* 2001; 11(6).
3. Lebas R, Menard T, Beau PA et al. Numerical simulation of primary break-up and atomization: DNS and modelling study. *International Journal of Multiphase Flow* 2009; 35(3): 247–260.
4. Chesnel J, Reveillon J and Demoulin FX. Large Eddy Simulation of Liquid Jet Atomization. *Atomization and Sprays* 2012; 21(9): 711–736.
5. Navarro-Martinez S. Large eddy simulation of spray atomization with a probability density function method. *International Journal of Multiphase Flow* 2014; 63: 11–22.
6. Richards KJ, Senecal PK and Pomraning E. Converge 2.3 Documentation. Technical report.
7. Jasak H, Jemcov A, Tukovic Z et al. Openfoam: A c++ library for complex physics simulations. In *International workshop on coupled methods in numerical dynamics*, volume 1000. IUC Dubrovnik, Croatia, pp. 1–20.
8. Strek P, Duke D, Swantek A et al. X-ray radiography and cfd studies of the spray g injector. SAE Technical Paper 2016-01-0858.
9. Saha K, Som S, Battistoni M et al. Numerical investigation of two-phase flow evolution of in- and near-nozzle regions of a gasoline direct injection engine during needle transients. *SAE Int J Engines* 2016; 9.
10. Saha K, Quan S, Battistoni M et al. Coupled eulerian internal nozzle flow and lagrangian spray simulations for GDI systems. SAE Technical Paper 2017-01-0834.
11. Allocca L, Bartolucci L, Cordiner S et al. ECN Spray G injector: Assessment of numerical modeling accuracy. SAE Technical Paper 2018-01-0306.
12. Saha K, Srivastava P, Quan S et al. Modeling the dynamic coupling of internal nozzle flow and spray formation for gasoline direct injection applications. SAE Technical Paper 2018-01-0314.
13. Baldwin E, Grover R, Parrish S et al. String flash-boiling in gasoline direct injection simulations with transient needle motion. *International Journal of Multiphase Flow* 2016; 87: 90 – 101.
14. Duret B, Reveillon J, Menard T et al. Improving primary atomization modeling through DNS of two-phase flows. *International Journal of Multiphase Flow* 2013; 55: 130–137.
15. Beheshti N, Burluka AA and Fairweather M. Assessment of ΣY liq model predictions for air-assisted atomisation. *Theoretical and Computational Fluid Dynamics* 2007; 21(5): 381–397.
16. Pandal Blanco A. *Implementation and Development of an Eulerian Spray Model for CFD simulations of diesel Sprays*. Phd, Univesitat Politecnica de Valencia, 2016.
17. Schmidt D, Gopalakrishnan S and Jasak H. Multi-dimensional simulation of thermal non-equilibrium channel flow. *International Journal of Multiphase Flow* 2010; 36(4): 284 – 292.
18. Valiño L. A field monte carlo formulation for calculating the probability density function of a single scalar in a turbulent flow. *Flow, Turbulence and Combustion* 1998; 60(2): 157–172.
19. ECN Workshop. Spray G ECN, Sandia National Laboratory, ecn.sandia.gov, 2015.
20. Issa RI, Gosman AD and Watkins AP. The computation of compressible and incompressible recirculating flows by a non-iterative implicit scheme. *Journal of Computational Physics* 1986; 62: 66–82.
21. Pomraning E and Rutland CJ. Dynamic one-equation nonviscosity large-eddy simulation model. *AIAA Journal* 2002; 40: 689–701.
22. Nicoud F and Ducros F. Subgrid-scale stress modelling based on the square of the velocity gradient tensor. *Flow, Turbulence and Combustion* 1999; 62(3): 183–200.
23. Tretola G, Vogiatzaki K and Navarro-Martinez S. Sub-grid effects in atomisation process using stochastic fields. In *ICLASS : 14th International Conference on Liquid Atomization and Spray Systems, Chicago, IL, USA*.
24. Duke D, Kastengren A, Matusik K et al. Internal and near nozzle measurements of Engine Combustion Network Spray G gasoline direct injectors. *Experimental Thermal and Fluid Science* 2017; 88: 608–621.
25. Beale C and Reitz RD. Modeling spray atomization with the kelvin-helmholtz/rayleigh-taylor hybrid model. *Atomization and Sprays* 1999; 9(4): 623 – 650.